Research Article

Shaoqiang Meng, Xiaowei Ouyang*, Jiyang Fu*, Yanfei Niu, and Yuwei Ma*

The role of graphene/graphene oxide in cement hydration

https://doi.org/10.1515/ntrev-2021-0055
received May 12, 2021; accepted July 16, 2021

Abstract: Graphene (G) and graphene oxide (GO) have been shown to significantly improve the mechanical properties of cement-based materials. In this study, the effect of the G/GO on cement hydration was investigated. First, the zeta potential of G/GO in simulated solutions was tested, and the interaction between G/GO's surface and Ca^{2+} was explored. Subsequently, scanning electron microscopy was used to observe the morphology of C–S–H nucleation and growth on the cement surface in the cement paste containing G/GO. Furthermore, XRD and TGA analyses were carried out on the hydration products of the sample. At last, isothermal calorimetry was applied to investigate the influence of G/GO on the early hydration of cement. The results showed that the addition of G/GO significantly accelerates C–S–H nucleation and growth on the cement surface. It is indicated that the high mobility ions derived by G/GO in the cement paste dominate the reason for the accelerated hydration of cement. The presence of G, especially GO, facilitates the mobility of ions, especially Ca^{2+}, thus enhances the interaction between the cement surface and the ions. This strong interaction promotes the C–S–H nucleation and growth, and therefore, the hydration of the cement.

Keywords: graphene, graphene oxide, cement paste, hydration, C–S–H, calcium ion

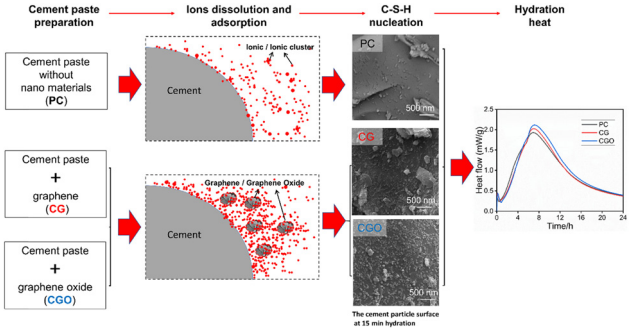

Graphical abstract: (1) GO has a strong interaction with Ca^{2+}. (2) G/GO accelerates C–S–H growth. (3) High mobility ions derived by G/GO facilitate hydration.

1 Introduction

Cement-based materials modified with nanomaterials can gain a significant performance improvement and related research has been receiving increasing attention [1–3]. Graphene (G) and graphene oxide (GO) are applied to optimize the performance of cement-based materials due to their unique properties [4,5]. Many studies [6–8] reported that GO can significantly improve the compression strength of cement-based materials. It reported that adding 1.5 wt% of GO increased the compressive strength by 53% [9]. Some studies [10–12] indicated that the change in compressive strength of G-modified cement-based materials is within 15%. However, Dela Vega and Vasquez [13] reported a 56% increase in compressive strength by adding 0.5 wt% of G.

The microstructure is the key to understanding the mechanical properties of cement-based materials. Liu *et al.* [14,15] reported a denser interfacial transition zone in mortars with G/GO, resulting in a significant increase in the strength. Zhang *et al.* [16] found that the porosity of GO-modified cement-based materials decreased by 31% at a GO content of 2.0 wt%. The improvement in microstructure and the decrease in porosity were attributed to the 'filling' and 'nucleation' effect of G/GO [17,18]. The addition of G/GO can not only refine the pore structure, but also regulate the formation of hydration products [19].

* **Corresponding author: Xiaowei Ouyang,** Research Center for Wind Engineering and Engineering Vibration, Guangzhou University, Guangzhou 510006, China, e-mail: xwouyang@gzhu.edu.cn
* **Corresponding author: Jiyang Fu,** Research Center for Wind Engineering and Engineering Vibration, Guangzhou University, Guangzhou 510006, China, e-mail: jyfu@gzhu.edu.cn
* **Corresponding author: Yuwei Ma,** Research Center for Wind Engineering and Engineering Vibration, Guangzhou University, Guangzhou 510006, China, e-mail: yuwei_ma@gzhu.edu.cn
Shaoqiang Meng: Research Center for Wind Engineering and Engineering Vibration, Guangzhou University, Guangzhou 510006, China, e-mail: 2111916027@e.gzhu.edu.cn
Yanfei Niu: School of Civil Engineering, Guangzhou University, Guangzhou 510006, China, e-mail: 525278741@qq.com

Open Access. © 2021 Shaoqiang Meng *et al.*, published by De Gruyter. This work is licensed under the Creative Commons Attribution 4.0 International License.

C–S–H is the most important hydration product [20]. Lu and Liu [21–23] found that the C–S–H becomes a regular flower in shape due to the nucleation and regulatory of G/GO in the formation of C–S–H. Wang *et al.* [24] reported that the incorporation of 0.01–0.05% GO accelerated the formation of C–S–H, and the arrangement of C–S–H was more regular. Most studies [25–27] reported that G/GO provides the C–S–H nucleation sites to enhance the cement hydration. In addition, Guo *et al.* [28–31] indicated that the interface of GO/C–S–H generates a new chemical bond. However, Kong *et al.* [32] did not find C–S–H on the surface of nanomaterials and believed that nanoparticles have no nucleation effect based on classical nucleation theory.

The effect of G/GO on cement hydration is still uncertain. These studies focused more on the morphology of C–S–H and less on the effect of G/GO on the formation process of C–S–H. The process of C–S–H formation is that the aggregations of ions or molecules become large and stable enough to develop nuclei in the saturated state and then grow gradually. G/GO has excellent electrical conductivity, which will motivate the ions in the solution [33]. The analysis of the effect of G/GO on the C–S–H morphology from the perspective of the C–S–H formation process would provide a deeper understanding of the role of G/GO in cement hydration.

Ca^{2+} plays an important role in the kinetic, morphological, and structural characteristics of C–S–H [34]. In this study, the interaction between G/GO and Ca^{2+} was first characterized with the zeta potential test. Then, SEM was applied to observe the hydrates in cement paste incorporating G/GO at 15 min, 1, 4, and 7 h of hydration. The hydration products of the samples were analyzed by XRD and TGA. Furthermore, isothermal calorimetry was used to measure the heat of cement hydration during the first 24 h. Finally, the role of G/GO in the early hydration of cement was discussed.

2 Materials

2.1 Materials and mixture

The materials used in this study include cement, G, and GO. The cement is Portland cement type I produced by Fushun Cement Co., Ltd. in China. The chemical content of the cement was tested by X-ray fluorescence (XRF), and the result is shown in Table 1. G/GO was purchased from Suzhou Carbon Fun Technology Co., Ltd. in China.

Table 1: Chemical content of cement (wt%)

CaO	SiO_2	Al_2O_3	Fe_2O_3	SO_3	MgO	K_2O	TiO_2	P_2O_5
63.51	20.86	5.3	3.56	2.67	1.81	0.631	0.387	0.332

The properties and characterization of G/GO are listed in Table 2. To further characterize G/GO, microscopic observation was performed by scanning electron microscopy (SEM) and the morphology of G/GO is shown in Figure 1. The red frame is the enlarged zone. The mixing ratio is detailed in Table 3. PC is a control sample with 100% cement paste. CG is a cement paste incorporating G. CGO is a cement paste containing GO.

2.2 Sample preparation

First, G/GO was added to water to produce a suspension of nanoscale particles. To disperse the G/GO uniformly in

Table 2: Physical parameters of G and GO

Types	Purity (wt%)	Thickness (nm)	Diameter of lamellae (nm)	Specific surface area (m^2/g)
G	>98	~2	5–10	1,000–1,217
GO	>95	~1	10–50	>400

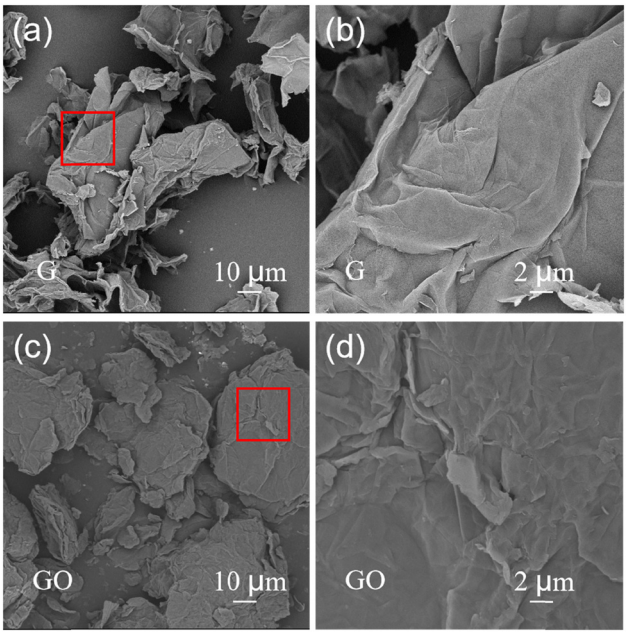

Figure 1: SEM image of G (a) and (b) and GO (c) and (d).

Table 3: Mix design

Sample code	Cement* (%)	Blending amount* (%)	w/b
PC	100	0	0.4
CG	100	0.4	0.4
CGO	100	0.4	0.4

*Percentage of the total mass of cement by weight.

the aqueous solution, the suspension was sonicated in an ultrasonic meter (Power of 400 W) for 15 min. Water temperature was controlled within 30°C in the sonicate process. Then, cement was put into the G/GO suspension and stirred evenly by a whisk at a slow speed for 2 min, then at a fast speed for 2 min. After that, all samples were placed in the standard conditioning chamber for 15 min, 1, 4, and 7 h, respectively. The samples were maintained to a specified age and then soaked in anhydrous ethanol to terminate the hydration. The samples in the anhydrous ethanol were filtered and dried in a 35°C oven for 12 h. Finally, the dried samples were collected for investigations.

2.3 Zeta potential test

The zeta potential of G/GO was tested with a Malvern Zetasizer Nano (Malvern Instruments Ltd., UK) in a simulated solution. The liquid phase of early cement pastes is mainly composed of Na^+, K^+, SO_4^{2-}, and Ca^{2+} ions. Ca^{2+} plays a key role in the cement hydration process [5,35,36]. Therefore, the $Ca(OH)_2$ solution was used as the simulated solution to measure the zeta potential of the G/GO. The preparation process of the $Ca(OH)_2$ solution can be found in the literature [36]. The measurements were repeated three times for each sample, and the average value was taken as the recorded value.

2.4 SEM

Before SEM observation, the conductive film was attached to the sample stage, and then each specimen (about 1 g) was fixed on the conductive film. To keep the sample stably fixed on the conductive film, it was sprayed with high-pressure gas. Due to the poor conductivity of the hardened paste, the powder samples were sprayed with gold before the test. Then, the samples were observed using a Phenom ProX electron microscope (Phenom, FEI). The specific details of this test method can be found in the literature [37].

2.5 X-ray diffraction (XRD)

An X-ray diffractometer (Japan Smartlab) was used to analyze the hydrated products of the samples. The radiation of the test was CuKα, the voltage was 40 kV, and the current was 40 mV. The diffraction angle was 10–80° with a step of 2°/min. The target material was copper. The samples were kept dry in a vacuum until testing.

2.6 Thermogravimetric (TGA)

TGA analysis of the samples was carried out by a term synchronous thermal analyzer (Germany NETZSCH-STA449F5). The set temperature rise rate was 10°C/min and the maximum temperature was 800°C. Argon was used as a protective gas. The $Ca(OH)_2$, $CaCO_3$, and C–S–H contents were calculated by the following equation [38]:

$$\text{LOI(CH)}(\%) = \frac{\text{Ca(OH)}_2 \text{ mass loss from 400 to 500°C}}{\text{sample mass at 800°C}} \times 100 \quad (1)$$

$$\text{LOI(CC)}(\%) = \frac{\text{CaCO}_3 \text{ mass loss from 600 to 700°C}}{\text{sample mass at 800°C}} \times 100 \quad (2)$$

$$\text{LOI(C–S–H)}(\%) = \text{mass loss from 105 to 800° C} - \text{LOI(CH)} - \text{LOI(CC)} \quad (3)$$

Note: LOI(CH) is the percentage of $Ca(OH)_2$ losing H_2O in the TG curve. LOI(CC) is the percentage of $CaCO_3$ losing CO_2 in the TG curve. LOI(C–S–H) is the percentage of the C–S–H losing H_2O in the TG curve.

2.7 Isothermal calorimetry

The exothermic rate of hydration and the total exothermic heat of hydration of samples were automatically measured and recorded by the TAM Air eight-channel isothermal calorimeter. The instrument temperature was set to 20°C, and the next step was performed after the instrument temperature stabilized. Ampoules containing samples were placed in the channel and the exothermic hydration data

were tested continuously for 24 h. Each recorded value was derived from the average of two measurement results.

3 Results and discussion

3.1 Zeta potential

The variation pattern of zeta potential of G/GO with Ca^{2+} concentration in $Ca(OH)_2$ solution is shown in Figure 2. The variation pattern of zeta potential for limestone powder (LP) and quartz powder (QP) in $Ca(OH)_2$ solution with Ca^{2+} concentration was tested by Ouyang *et al.* [36]. This result was compared with the zeta potential of C–S–H particles measured by Nachbaur *et al.* [39] and Viallis-Terrisse *et al.* [40]. As can be seen from Figure 2, for a certain Ca^{2+} concentration, the zeta potentials of QP and C–S–H particles were similar, while the zeta potentials of LP particles were relatively more positive. LP particles have stronger interaction with Ca^{2+} compared to QP and C–S–H particles [36].

As can be seen from Figure 2, the zeta potential of G is –15.3 mV at a Ca^{2+} concentration of 0.2 mmol/L. With the increase of Ca^{2+} concentration, the zeta potential of G is almost linear and increases due to the adsorption of Ca^{2+} on particles' surfaces. The isoelectric point (IEP) corresponds to a point where the zeta potential is 0, indicating that the electrophoretic mobility is 0. G particles reach IEP at a Ca^{2+} concentration of about 2 mmol/L, which is similar to QP and C–S–H particles. The potential value of G is positive after a Ca^{2+} concentration of about 2 mmol/L. And the maximum value of the potential of G is 24.55 mV at a Ca^{2+} concentration of 6 mmol/L. In general, the trend

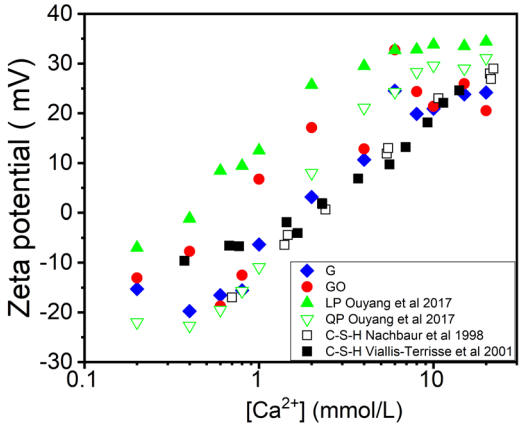

Figure 2: The variation pattern of zeta potential of G, GO, LP, QP, and C–S–H particles with Ca^{2+} concentration in $Ca(OH)_2$ solution.

of the potential of G with Ca^{2+} concentration is similar to that of QP and C–S–H. It is indicated that G particles have similar interaction with Ca^{2+} as QP and C–S–H particles.

For GO particles, the potential of suspension exhibits a negative value at a Ca^{2+} concentration of 0.2 mmol/L. It may be caused by carboxylate groups on the surface [41]. GO particles reach IEP at a Ca^{2+} concentration of below 2 mmol/L, which is about 0.9 mmol/L. The zeta potential increased with increasing Ca^{2+} concentration from 0.9 to 6 mmol/L. The maximum value of potential is 32.77 mV at a Ca^{2+} concentration of 6 mmol/L. After Ca^{2+} concentration continued to increase, the high concentration solution of Ca^{2+} resulted in an irregular decrease of G/GO potential [42]. The potential of GO is higher than that of G, QP, and C–S–H for the same Ca^{2+} concentration. It is possible due to the oxygen-containing groups which have a stronger interaction with Ca^{2+} [41].

3.2 Morphology of hydrates

Figure 3 presents the SEM image of hydration products on the surface of cement particles at 15 min and 1 h hydration. The red frame is the enlarged zone. SEM image of the surface of cement particles in PC paste after hydration for 15 min is shown in Figure 3a and b (partial enlarged). It can be seen that some rod-shaped C–S–H particles appear on cement surface. Figure 3c and d (partial enlarged) demonstrate that many needle-shaped C–S–H particles are distributed on the surface of cement particles in CG paste after hydration for 15 min. The surface of cement particles is covered by C–S–H of similar dimensions in CGO paste after hydration for 15 min (Figure 3e and f). For CG and CGO past, the C–S–H on the cement surface appears denser and more uniform than that in PC paste. In addition, as can be observed in Figure 3d and f, the C–S–H on the surface of cement particles in the CGO paste is larger and a little denser than that in CG paste.

In Figure 3g and h, the size of the rod-shaped C–S–H started to grow on the surface of cement particles in PC paste after hydration for 1 h. As can be observed from Figure 3i and j, the surface of cement particles in CG paste has needle-shaped C–S–H after hydration for 1 h. These C–S–H were numerous and evenly distributed. Figure 3k and l (partial enlarged) also show a large number of needle-shaped C–S–H covering on the surface of cement particles in CGO paste after hydration for 1 h. Compared to PC paste, the surface of cement particles has more and finer needle-shaped C–S–H in CG and CGO paste.

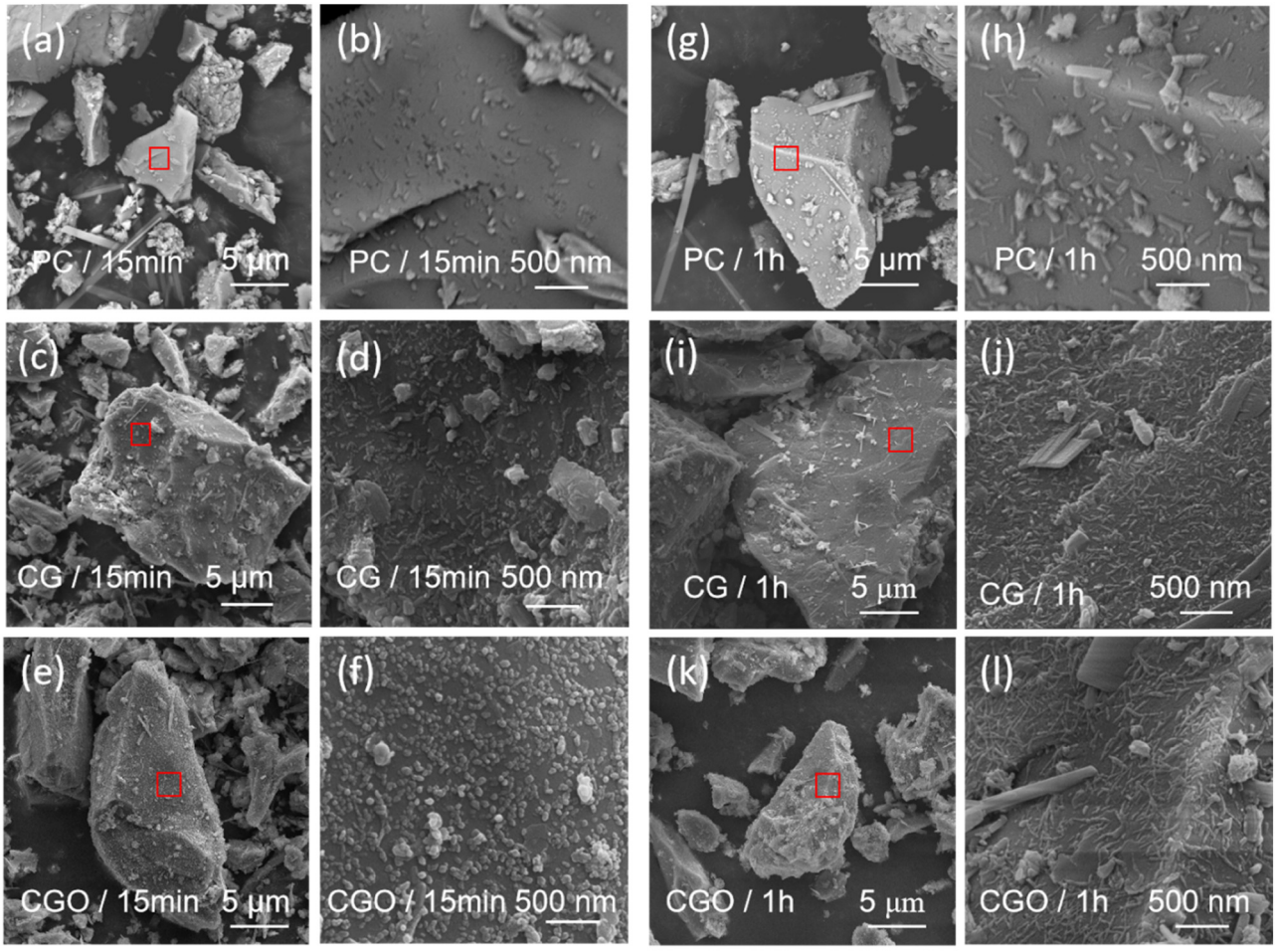

Figure 3: Morphology of hydration products on the surface of cement particles at 15 min in PC (a and b), CG (c and d), CGO (e and f), and at 1 h in PC (g and h), CG (i and j), CGO (k and l).

Figure 4 presents the morphology of hydration products on the surface of cement particles at 4 and 7 h. As can be seen in Figure 4a and b, some rod-shaped C–S–H particles become larger on the surface of cement particles in PC paste after hydration for 4 h. The size is still not uniform. As shown in Figure 4c and d (partial enlarged), there are a large number of fine C–S–H and some calcium hydroxide (CH) particles on the surface of cement particles in CG paste after hydration for 4 h. Meanwhile, many fine C–S–H particles on the surface of cement particles were also observed in CGO paste after hydration for 4 h. These results show that the C–S–H on the surface of cement particles in CG and CGO is finer and has more quantity than that in PC paste.

As demonstrated in Figure 4g and h (partial enlarged), overlapping rod-shaped C–S–H can be identified and their growth orientation is varied on the surface of cement particles in PC paste after hydration for 7 h. Figure 4i and j (partial enlarged) show that the mesh structure formed by the interweaving of C–S–H completely covers the surface of cement particles in CG paste. As can be observed from Figure 4k and l (partial enlarged), the surface of cement particles is also covered by the C–S–H of the mesh structure after hydration for 7 h. The difference in the morphology of C–S–H between the PC paste and CG and CGO paste is significant. Compared to PC paste, C–S–H with a higher amount and finer dimensions appears on the surface of cement particles in CG and CGO paste.

3.3 XRD analysis

XRD data are shown in Figure 5, mainly identifying C_2S, C_3S, CH, and $CaCO_3$. CG and CGO pastes do not show significantly different diffraction peaks. This indicates that the addition of G/GO to the cement paste does not produce new substances. The diffraction peaks of CH do

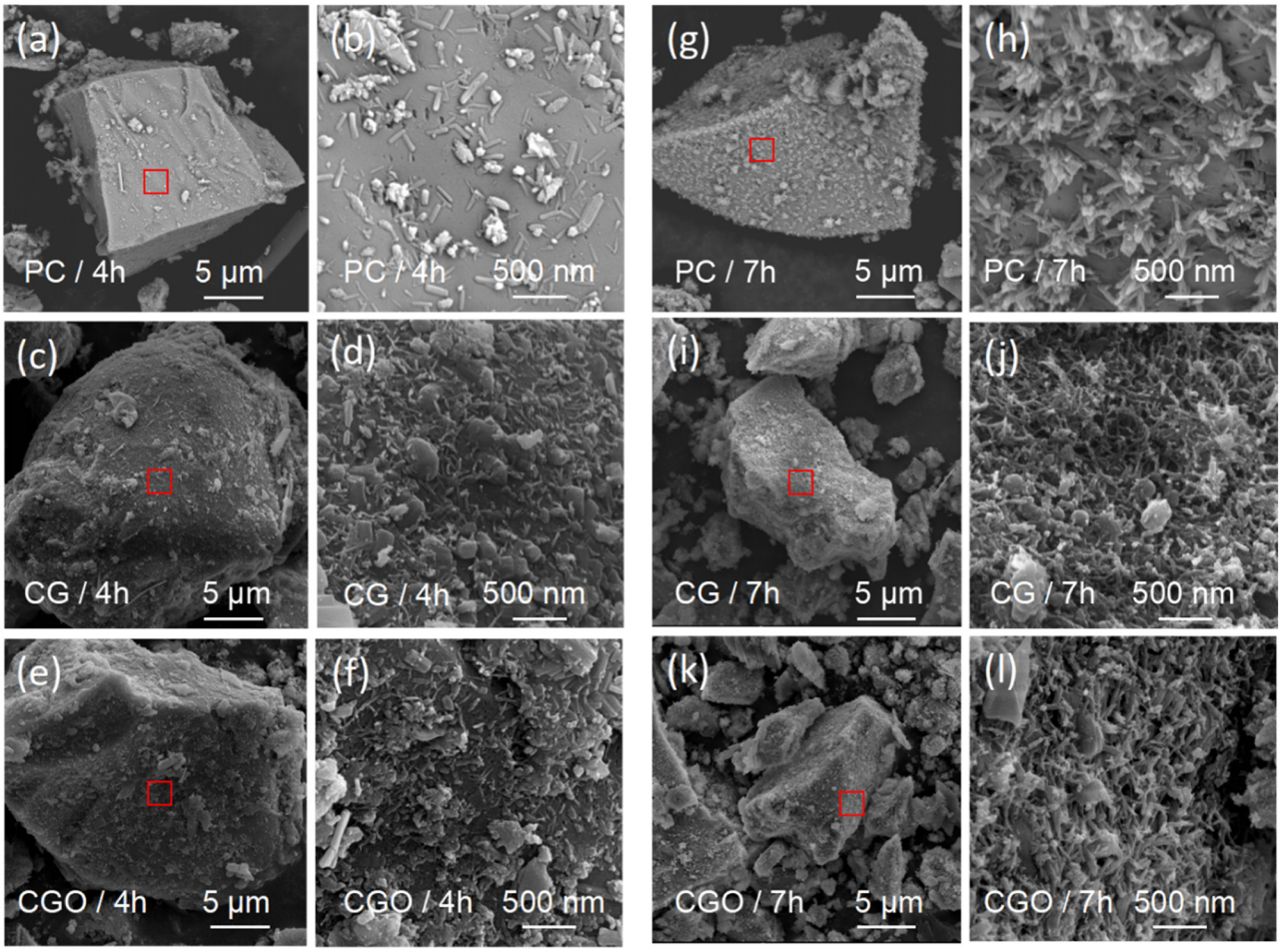

Figure 4: Morphology of hydration products on the surface of cement particles at 4 h in PC (a and b), CG (c and d), CGO (e and f), and at 7 h in PC (g and h), CG (i and j), CGO (k and l).

not change significantly after the addition of G/GO. However, the diffraction peak of $CaCO_3$ was found. It is possible due to the carbonation of $Ca(OH)_2$.

3.4 TGA analysis

The TG and DTG curves of PC, CG, and CGO obtained by TGA analysis are presented in Figure 6. The weight loss at 50–105°C is caused by the evaporation of adsorbed water. The weight loss at 110–170°C is caused by dehydration of the gel phase, such as AFt, C–S–H, *etc*. The weight loss at 400–500°C and 600–700°C is caused by the dehydration of $Ca(OH)_2$ and the decomposition of $CaCO_3$. The presence of $CaCO_3$ suggests that the $Ca(OH)_2$ was carbonized, verifying the XRD results.

The hydration degree of the sample can be quantified by the content of $Ca(OH)_2$, $CaCO_3$, and C–S–H. The contents of $Ca(OH)_2$, $CaCO_3$, and C–S–H were calculated and shown in Figure 7. It can be seen that the total contents of $Ca(OH)_2$, $CaCO_3$ in the CG and CGO pastes are higher than those in the PC paste. Moreover, the content of C–S–H in CG and CGO pastes was higher than that in PC pastes. It further indicates that the addition of G/GO can promote the hydration of cement, and thus generate more hydration products at the same hydration time. The content of C–S–H in the CGO paste is significantly less than that in CG in Figure 7(d). It is most likely due to partial C–S–H filtered out in the sample preparation.

3.5 Cement hydration heat calorimetry analysis

Figure 8 shows the exothermic rate and total accumulated heat obtained from the isothermal calorimetry test. The exothermic rate of hydration is presented in Figure 8a. It can be found that the induction period of CG/CGO paste is

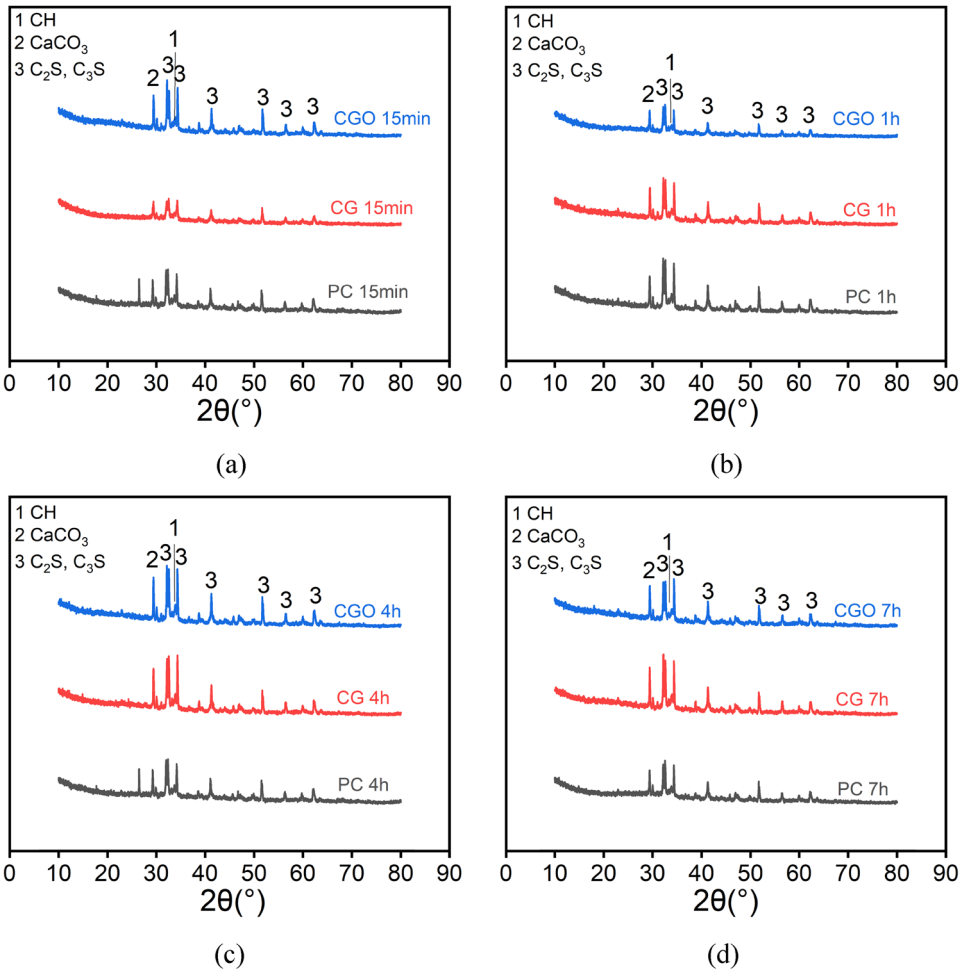

Figure 5: XRD patterns of the sample at 15 min (a), 1 h (b), 4 h (c), and 7 h (d).

longer than PC paste. The peak of heat flow for PC, CG, and CGO paste is 1.93, 2.02, and 2.11 mW/g, respectively. Peak heat flow increased by 5.1% and 9.8% for CG and CGO pastes, respectively, compared to PC pastes. The data obtained indicate that the presence of G/GO significantly facilitates the exothermic rate of cement hydration. The total accumulated heat of hydration is demonstrated in Figure 8b. At 24 h of hydration, the total accumulated heat of PC, CG, and CGO paste is 84.57, 85.10, and 89.64 J/g, respectively. The total accumulated heat for CG and CGO pastes increased by 0.63% and 6.0%, respectively, compared to PC pastes. These data show that the incorporation of GO accelerates the hydration of the cement paste. However, the total accumulated heat of CG paste is similar to that of PC paste. Similar results have been found in previous studies [18,43].

3.6 Discussion

The formation of C–S–H undergoes the process of nucleation and growth [44]. Classical theory suggests that nucleation and growth are related to the concentration of ions and are dynamic equilibrium processes of dissolution and recrystallization of cement particles [45]. The steps are as follows: (1) cement in solution dissolves a large number of ions. Due to irregular motion or interatomic attraction, ions move to the matrix surface and are adsorbed to form ion clusters (nuclei). (2) Ionic clusters may adsorb surrounding ions and grow. These ion clusters will continue to grow until their size exceeds the limit of the critical range. After that, the nuclei will enter the growth process. (3) Before reaching critical clusters, the ion clusters may also dissolve and reenter the solution [46]. After that step (1) is repeated.

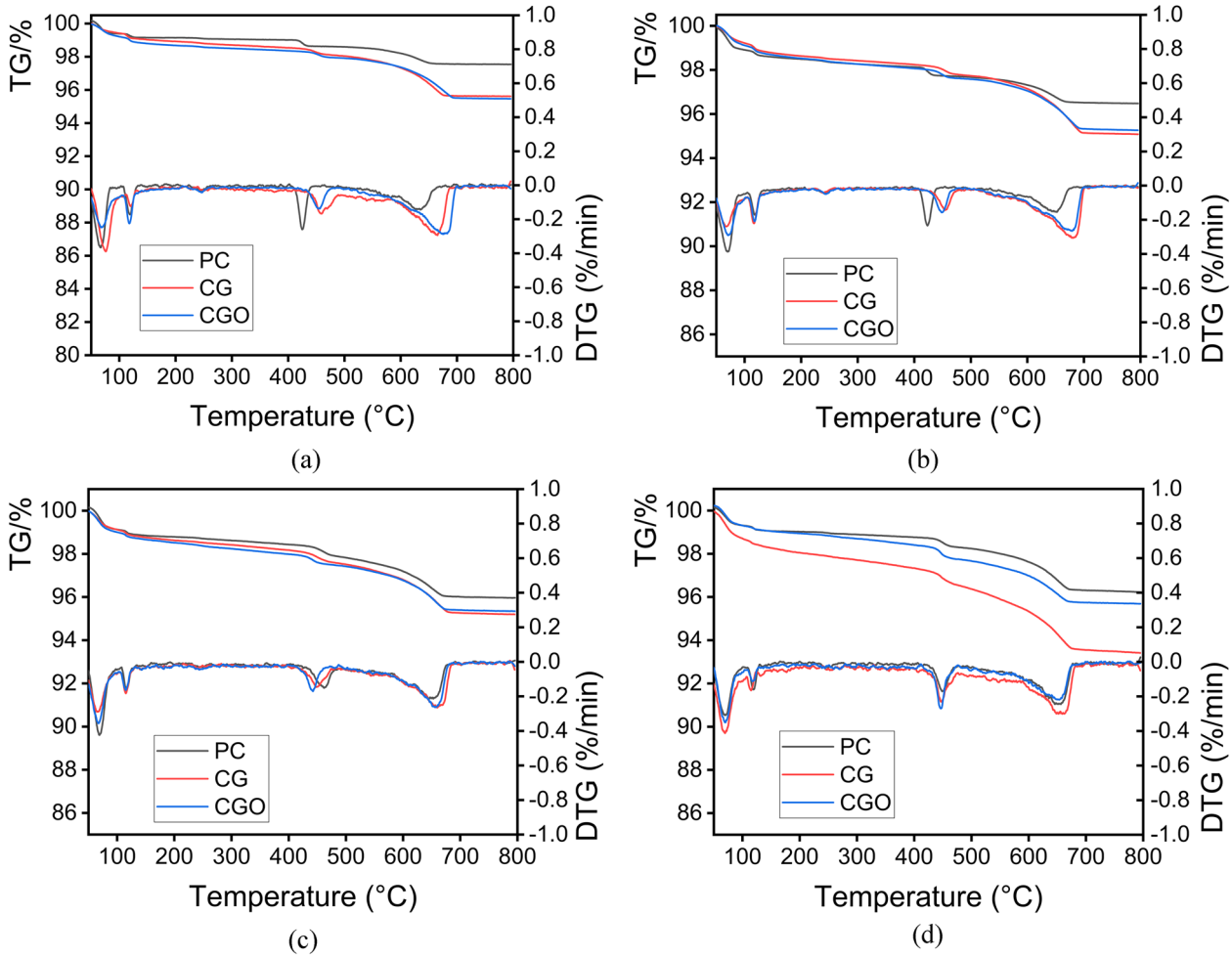

Figure 6: TG-DTG analyses of PC, CG, and CGO pastes at 15 min (a), 1 h (b), 4 h (c), and 7 h (d).

When cement comes in contact with water, the cement dissolves, releasing large amounts of ions. Ca^{2+} ions are soon absorbed on the surface of G/GO, increasing zeta potential value. As described in the previous section 3.1, G particles adsorb a large amount of Ca^{2+} on their surface, while the adsorption of Ca^{2+} ions on the surface of GO particles is higher than that of G, QP, and C–S–H particles. After a while, the Ca^{2+} concentration in the vicinity of G/GO gradually increased. With a high surface area and strong affinity to Ca^{2+}, G/GO can greatly promote the mobility of ions in cement paste, facilitating the development of ionic clusters and thus generating a large quantity of needle-shaped C–S–H particles at the cement surface, as demonstrated in Figures 3 and 4. Many studies [11,14,25–27,47,48] have suggested that the high surface area of G/GO may provide additional sites for C–S–H nucleation, enhancing the nucleation effect, thus facilitating the hydration process. However, the nucleation effect on the G/GO surface is difficult to be observed experimentally. In this study, the high-density C–S–H covered on the surface of cement particles in CG/CGO paste is not due to the nucleation effect of G/GO. This is possible because G/GO increases the mobility of ions in cement paste, which greatly increases the interaction of Ca^{2+} with the surface of cement particles, thus promoting the nucleation and growth process of C–S–H on cement surface. In other words, the high mobility ions derived by G/GO in the cement paste dominate the reason for the accelerated hydration of cement.

4 Conclusions

(1) The zeta potential of G is similar to QP and C–S–H particles in $Ca(OH)_2$ solutions. The higher zeta potential of GO indicates a stronger interaction between the GO surface and the Ca^{2+} ions.

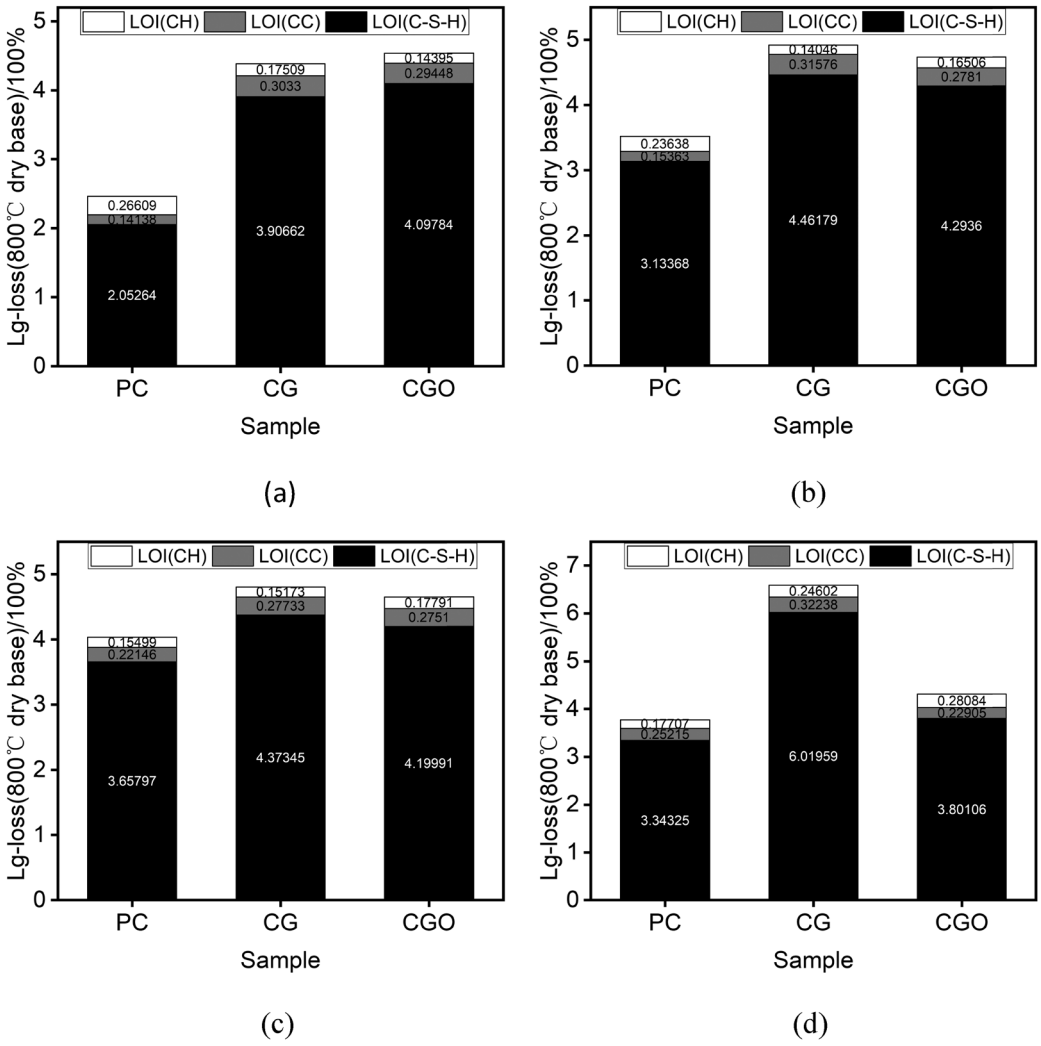

Figure 7: The relative content of the hydration products of the samples at 15 min (a), 1 h (b), 4 h (c), and 7 h (d).

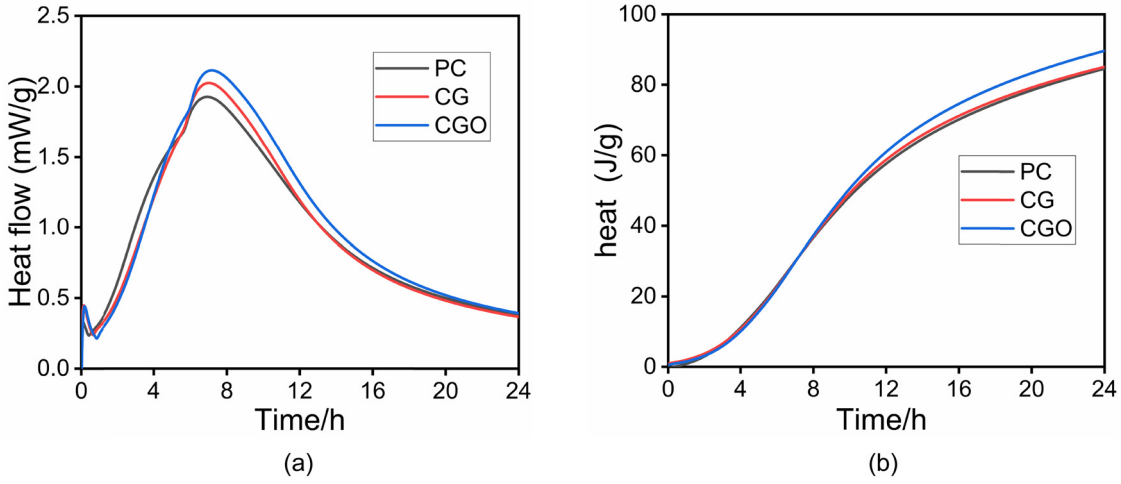

Figure 8: The heat flow (a) and accumulated heat (b) of PC, CG, and CGO pastes.

(2) The C–S–H on the surface of cement particles in CG and CGO past is denser and more uniform than that in PC paste at the same hydration time.
(3) The exothermic peak value in CG and CGO paste is 5.1 and 9.8% higher than that in PC paste. The total accumulation exothermic of CGO paste was 6.0% higher than that of PC paste.
(4) The presence of G, especially GO, facilitates the mobility of ions, especially Ca^{2+}, and thus enhances the interaction between the cement surface and the ions. This strong interaction promotes the C–S–H nucleation and growth, and therefore, the hydration of the cement.

Funding information: The authors would like to acknowledge the financial support from the National Nature Science Foundation of China (Grant No. 51925802 and 52008119), the Natural Science Foundation of Guangdong Province (Grant No. 2019A1515110799 and 2021A1515012624), and the 111 Project (Grant No. D21021).

Author contributions: All authors have accepted responsibility for the entire content of this manuscript and approved its submission.

Conflict of interest: The authors state no conflict of interest.

References

[1] Zhao Z, Qi T, Zhou W, Hui D, Xiao C, Qi J, et al. A review on the properties, reinforcing effects, and commercialization of nanomaterials for cement-based materials. Nanotechnol Rev. 2020;9(1):303–22.
[2] Liew KM, Kai MF, Zhang MW. Carbon nanotube reinforced cementitious composites: an overview. Compos Part A Appl Sci Manufact. 2016;91(1):301–23.
[3] Fouaidi M, Jamal M, Zaite A, Belouaggadia N. Bending analysis of functionally graded graphene oxide powder-reinforced composite beams using a meshfree method. Aerosp Sci Technol. 2021;110:106479–80.
[4] Yan Y, Nashath FZ, Chen S, Manickam S, Lim SS, Zhao H, et al. Synthesis of graphene: potential carbon precursors and approaches. Nanotechnol Rev. 2020;9(1):1284–314.
[5] Scrivener K, Ouzia A, Juilland P, Kunhi Mohamed A. Advances in understanding cement hydration mechanisms. Cem Concr Res. 2019;124:105823.
[6] Wang J, Xu Y, Wu X, Zhang P, Hu S. Advances of graphene- and graphene oxide-modified cementitious materials. Nanotechnol Rev. 2020;9(1):465–77.
[7] Zhao L, Guo XL, Song L, Song Y, Dai GZ, Liu JP. An intensive review on the role of graphene oxide in cement-based materials. Constr Build Mater. 2020;241(2020):117939.
[8] Zhao Y, Liu Y, Shi T, Gu Y, Zheng B, Zhang K, et al. Study of mechanical properties and early-stage deformation properties of graphene-modified cement-based materials. Constr Build Mater. 2020;257:119498–507.
[9] Gopalakrishnan R, Kaveri R. Using graphene oxide to improve the mechanical and electrical properties of fiber-reinforced high-volume sugarcane bagasse ash cement mortar. Eur Phys J Plus. 2021;136(2):1–15.
[10] Liu Q, Wu W, Xiao J, Tian Y, Chen J, Singh A. Correlation between damage evolution and resistivity reaction of concrete in-filled with graphene nanoplatelets. Constr Build Mater. 2019;208:482–91.
[11] Krystek M, Pakulski D, Patroniak V, Gorski M, Szojda L, Ciesielski A, et al. High-performance graphene-based cementitious composites. Adv Sci (Weinh). 2019;6(9):1801195–210.
[12] Ying G-G, Song C, Ren J, Guo S-Y, Nie R, Zhang L. Mechanical and durability-related performance of graphene/epoxy resin and epoxy resin enhanced OPC mortar. Constr Build Mater. 2021;282:122644–59.
[13] Dela Vega MSDC, Vasquez MR. Plasma-functionalized exfoliated multilayered graphene as cement reinforcement. Compos Part B Eng. 2019;160:573–85.
[14] Liu C, Huang X, Wu Y-Y, Deng X, Zheng Z. The effect of graphene oxide on the mechanical properties, impermeability and corrosion resistance of cement mortar containing mineral admixtures. Constr Build Mater. 2021;288:123059–73.
[15] Pei C, Ueda T, Zhu J. Investigation of the effectiveness of graphene/polyvinyl alcohol on the mechanical and electrical properties of cement composites. Mater Struct. 2020;53(3):1–15.
[16] Zhai S, Pang B, Liu G, Zhang Y, Xu K, She W, et al. Investigation on preparation and multifunctionality of reduced graphene oxide cement mortar. Constr Build Mater. 2021;275:122119–32.
[17] Wang B, Pang B. Mechanical property and toughening mechanism of water reducing agents modified graphene nanoplatelets reinforced cement composites. Constr Build Mater. 2019;226:699–711.
[18] Baomin W, Shuang D. Effect and mechanism of graphene nanoplatelets on hydration reaction, mechanical properties and microstructure of cement composites. Constr Build Mater. 2019;228:116720.
[19] Indukuri CSR, Nerella R. Enhanced transport properties of graphene oxide based cement composite material. J Build Eng. 2021;37:102174.
[20] Pellenq RJM, Van Damme H. Why does concrete set? The nature of cohesion forces in hardened cement-based materials. MRS Bull. 2011;29(5):319–23.
[21] Liu Y, Jia M, Song C, Lu S, Wang H, Zhang G, et al. Enhancing ultra-early strength of sulphoaluminate cement-based materials by incorporating graphene oxide. Nanotechnol Rev. 2020;9(1):17–27.
[22] Wang L, Li Q, Song J, Liu S. Effect of graphene oxide on early hydration and compressive strength of Portland cement-copper tailing powder composite binder. Powder Technol. 2021;386:428–36.

[23] Chintalapudi K, Pannem RMR. The effects of graphene oxide addition on hydration process, crystal shapes, and microstructural transformation of ordinary portland cement. J Build Eng. 2020;32:101551–61.
[24] Wang Q, Wang J, Lu CX, Liu BW, Zhang K, Li CZ. Influence of graphene oxide additions on the microstructure and mechanical strength of cement. Carbon. 2015;95:1083–4.
[25] Ho VD, Ng C-T, Ozbakkaloglu T, Goodwin A, McGuckin C, Karunagaran RU, et al. Influence of pristine graphene particle sizes on physicochemical, microstructural and mechanical properties of Portland cement mortars. Constr Build Mater. 2020;264(2020):120188–200.
[26] Ho VD, Ng C-T, Ozbakkaloglu T, Karunagaran RU, Farivar F, Goodwin A, et al. Investigating the reinforcing mechanism and optimized dosage of pristine graphene for enhancing mechanical strengths of cementitious composites. RSC Adv. 2020;10(70):42777–89.
[27] Yan S, Yan S, Tang J, Wang X. Effect of graphene on the mechanical properties of the cement paste. J Appl Mech Tech Phys. 2020;61(6):972–8.
[28] Zhao L, Guo X, Liu Y, Zhao Y, Chen Z, Zhang Y, et al. Hydration kinetics, pore structure, 3D network calcium silicate hydrate, and mechanical behavior of graphene oxide reinforced cement composites. Constr Build Mater. 2018;190:150–63.
[29] Wan H, Zhang Y. Interfacial bonding between graphene oxide and calcium silicate hydrate gel of ultra-high performance concrete. Mater Struct. 2020;53(2):1–12.
[30] Fan D, Yang S, Saafi M. Molecular dynamics simulation of mechanical properties of intercalated GO/C–S–H nanocomposites. Comput Mater Sci. 2021;186:110012–23.
[31] Wang P, Qiao G, Hou D, Jin Z, Wang M, Zhang J, et al. Functionalization enhancement interfacial bonding strength between graphene sheets and calcium silicate hydrate: Insights from molecular dynamics simulation. Constr Build Mater. 2020;261:120500–9.
[32] Kong D, Huang S, Corr D, Yang Y, Whether SPShah. do nanoparticles act as nucleation sites for C–S–H gel growth during cement hydration. Cem Concr Compos. 2018;87:98–109.
[33] Alamdarlo FV, Solookinejad G, Zahakifar F, Jalal MR, Jabbari M. Study of kinetic, thermodynamic, and isotherm of Sr adsorption from aqueous solutions on graphene oxide (GO) and (aminomethyl)phosphonic acid–graphene oxide (AMPA–GO). J Radioanal Nucl Chem. 2021;329:1033–43.
[34] Garrault-Gauffinet S, Nonat A. Experimental investigation of calcium silicate hydrate (C–S–H) nucleation. J Cryst Growth. 1999;200(3/4):565–74.
[35] Ouyang X, Koleva DA, Ye G, van Breugel K. Understanding the adhesion mechanisms between C–S–H and fillers. Cem Concr Res. 2017;100:275–83.
[36] Ouyang X, Koleva DA, Ye G, van Breugel K. Insights into the mechanisms of nucleation and growth of C–S–H on fillers. Mater Struct. 2017;50(5):213.
[37] Ouyang X, Wang L, Fu J, Xu S, Ma Y. Surface properties of clay brick powder and its influence on hydration and strength development of cement paste. Constr Build Mater. 2021;300(7):123958.
[38] Aono Y, Matsushita F, Shibata S, Hama Y. Nano-structural changes of C–S–H in hardened cement paste during drying at 50°C. J Adv Concr Technol. 2007;5(3):313–23.
[39] Nachbaur L, Nkinamubanzi P-C, Nonat A, Mutin JC. Electrokinetic properties which control the coagulation of silicate cement suspensions during early age hydration. J Colloid Interface Sci. 1998;202:261–8.
[40] Viallis-Terrisse H, Nonat A, Petit JC. Zeta-potential study of calcium silicate hydrates interacting with alkaline cations. J Colloid Interface Sci. 2001;244(1):58–65.
[41] Park S, Ruoff RS. Chemical methods for the production of graphenes. Nat Nanotechnol. 2009;4(4):217–24.
[42] Ouyang X, Wang L, Xu S, Ma Y, Ye G. Surface characterization of carbonated recycled concrete fines and its effect on the rheology, hydration and strength development of cement paste. Cem Concr Compos. 2020;114:103809.
[43] Meng W, Khayat KH. Effect of graphite nanoplatelets and carbon nanofibers on rheology, hydration, shrinkage, mechanical properties, and microstructure of UHPC. Cem Concr Res. 2018;105:64–71.
[44] Goldberg SJGECA. Review of chemistry of the solid-water interface. Processes at the mineral-water and particle-water interface in natural systems, by Werner Stumm. J Colloid Interface Sci. 1992;57(3):205–19.
[45] Gauffinet S, Finot E, Nonat AJM. Structures, experimental study and simulation of C–S–H nucleation and growth. J Colloid Interface Sci. 1997;62(2):1–16.
[46] Vekilov PG. Nucleation. Cryst Growth Des. 2010;10(12):5007–19.
[47] Lin C, Wei W, Hu YH. Catalytic behavior of graphene oxide for cement hydration process. J Phys Chem Solids. 2016;89:128–33.
[48] Lu Z, Li X, Hanif A, Chen B, Parthasarathy P, Yu J, et al. Early-age interaction mechanism between the graphene oxide and cement hydrates. Constr Build Mater. 2017;152:232–9.